Intermetallics 132 (2021) 107133

Contents lists available at ScienceDirect

Intermetallics

journal homepage: http://www.elsevier.com/locate/intermet

Synergistic strengthening mechanisms of rhenium in nickel-based single crystal superalloys

En-Lai Yue [a], Tao Yu [a,*], Yun-Jiang Wang [b,c,**], Chong-Yu Wang [a,d,***]

[a] Central Iron and Steel Research Institute, Beijing, China
[b] State Key Laboratory of Nonlinear Mechanics, Institute of Mechanics, Chinese Academy of Sciences, Beijing, China
[c] School of Engineering Science, University of Chinese Academy of Sciences, Beijing, China
[d] Department of Physics, Tsinghua University, Beijing, China

ARTICLE INFO

Keywords:
A. Intermetallics
B. Plastic deformation mechanisms
B. Solid-solution hardening
D. Dislocation geometry and arrangement
E. Molecular dynamics simulation

ABSTRACT

A loading-unloading-reloading strategy via atomistic simulations is proposed to reveal the strengthening mechanisms of rhenium in nickel-based superalloys at ambient temperature. Simulations reproduce the experimentally observed increased flow stress with addition of rhenium. Besides the usual solid solution strengthening, two novel mechanisms are uncovered. One is that rhenium facilitates the dislocation nucleation and, thus, increases the propensity of forest dislocation interactions. The other involves a critical role of rhenium in promoting accumulation of sessile stair-rod dislocations, served as obstacles for the glissile dislocations. The three mechanisms synergistically render a stronger alloy, which is heuristic to design advanced superalloys in extreme environments.

1. Introduction

Nickel (Ni)-based single crystal (SC) superalloys are of unique structure consisting of a disordered solid solution γ-Ni matrix (face-centered cubic) and an ordered γ'-Ni_3Al ($L1_2$) precipitate. They are widely used in turbine blades of advanced aircraft engines [1–3], owing to their outstanding mechanical strength and, in particular, the enhanced creep resistance at elevated temperature. This superalloy usually contains more than ten alloying elements. Among them, the element rhenium (Re) plays an extremely important role in their high-temperature mechanics and creep performance [4–7]. As such the superalloys are usually categorized into a first (0 wt.% Re), second (2–4 wt.% Re) and third (5–7 wt.% Re) generation [8,9], respectively, according to the concentration of this element.

The enhancement in mechanical properties of Ni-based superalloys due to Re addition has been attributed to several mechanisms. First, as expected for the doping atom with large diameter, Re provides a high degree of solid solution strengthening and increases the flow stress of alloys [10]. Next, due to a sluggish diffusion of Re in Ni matrix [11–14], it can also slow down the motion of dislocations [15] and retard the coarsening of γ' phase [16,17]. Then the segregation of Re at the γ/γ' interfacial dislocation networks can further strengthen the interface and make the dislocation networks strong against the shear from mobile dislocations [18]. Finally, Re can reduce the creep rate in Ni-based SC superalloys by being enriched around the dislocation core and imposing a drag effect on the movement of dislocations [19]. However, a comprehensive atomic-scale strengthening mechanism of Re is rarely reported in Ni-based superalloys due to the difficulty of *in situ* characterization at microscopic of bulk materials.

Instead, atomistic simulations via molecular dynamics (MD) provide a complementary tool to survey the atomic-scale resolution dislocation behaviors under proper conditions of deformation. The deformation and fracture of the nanostructured Ni, Ni_3Al and model superalloys have been analyzed by MD down to the level of dislocation nucleation and evolution from surface or crack tip [20–24]. However, such simulations starting with a defect-free model usually suffer from the artificial stress overshoot at yielding which hinders a rational understanding of the mechanical performance from an atomistic perspective. To settle the issue, here we propose a loading-unloading-reloading technique based on MD, to mimic an experimentally relevant deformation condition, which extracts synergistic strengthening mechanisms of Re in Ni-based

* Corresponding author. Central Iron and Steel Research Institute, Beijing, China.
** Corresponding author. State Key Laboratory of Nonlinear Mechanics, Institute of Mechanics, Chinese Academy of Sciences, Beijing, China.
*** Corresponding author. Department of Physics, Tsinghua University, Beijing, China.
E-mail addresses: ytao012345@163.com (T. Yu), yjwang@imech.ac.cn (Y.-J. Wang), cywang@mail.tsinghua.edu.cn (C.-Y. Wang).

https://doi.org/10.1016/j.intermet.2021.107133
Received 25 August 2020; Received in revised form 3 January 2021; Accepted 5 February 2021
Available online 22 February 2021

superalloys, with combined roles of solid solution strengthening, extra dislocation proliferation, as well as the existence of sessile stair-rod dislocations.

2. Methodology

The MD simulations are performed by LAMMPS code [25] based on a 3D superalloy model including both γ phase and γ' phase, to mimic a real superalloy. Our recently developed multi-component Ni–Al-Re empirical potential in the embedded atom method (EAM) framework is adopted to describe the force field [26]. It has been widely used to study the segregation of Re [18,19], the interface crack propagation [27,28], as well as lattice trapping of Ni-based superalloys [29]. Note that the accuracy of all classical MD simulations depends on the reliability of an empirical potential. The present simulations are not exceptional. Therefore, the used Ni–Al-Re potential has been widely benchmarked by either experimental, or first-principles data, in terms of point and planar defect formation energies, stacking fault energy, anti-phase boundary, complex stacking fault and superlattice intrinsic stacking fault energies in both FCC-Ni, FCC-Al and HCP-Re, and $L1_2$-Ni_3Al. All the features are quite relevant to the dislocation and mechanical behavior of the Ni-based alloys. The atomic structure visualization and dislocation analysis are conducted by software OVITO [30]. The dislocation density is calculated as the length of dislocations in unit volume.

The scheme and geometry of the model setup are demonstrated in Fig. 1, which contains 2,475,820 atoms described by periodic boundary conditions along x[100], y[010] and z[001] directions, respectively. Due to the difference in lattice parameters between γ and γ' phases, proper lattice misfit is inevitable on the γ/γ' interface. The lattice misfit δ is defined as [31]:

$$\delta = \frac{2(a_{\gamma'} - a_{\gamma})}{a_{\gamma'} + a_{\gamma}} \tag{1}$$

where $a_{\gamma} = 3.520$ Å and $a_{\gamma'} = 3.567$ Å are the lattice parameters of γ-Ni and γ'-Ni_3Al phases, respectively, determined by the present EAM potential. Thus, the largest interface lattice misfit of the system is $\delta = 1.33\%$ under the condition of one-to-one unit cell of Ni and Ni_3Al. The interface strain can be optimized by changing the size of the model. For a superalloy model containing n Ni_3Al unit cells, and $n+1$ Ni unit cells, an optimal model satisfies the following relationship:

$$na_{\gamma'} = (n+1)a_{\gamma} \tag{2}$$

which yields $n \approx 75$. In this context we build a γ/γ' model with the dimension of $(86a_{\gamma})^3$, the inner part of which is of $(75a_{\gamma'})^3$ γ' block. The volume fraction of γ' phase in the superalloy model is $(75a_{\gamma'}/86a_{\gamma})^3 \approx 69\%$, which is comparable to experiment ~70% [32]. The total width of the model is 30.3 nm, in which the width of γ' phase is 26.8 nm, as shown in Fig. 1(a). Note that the present atomic model is

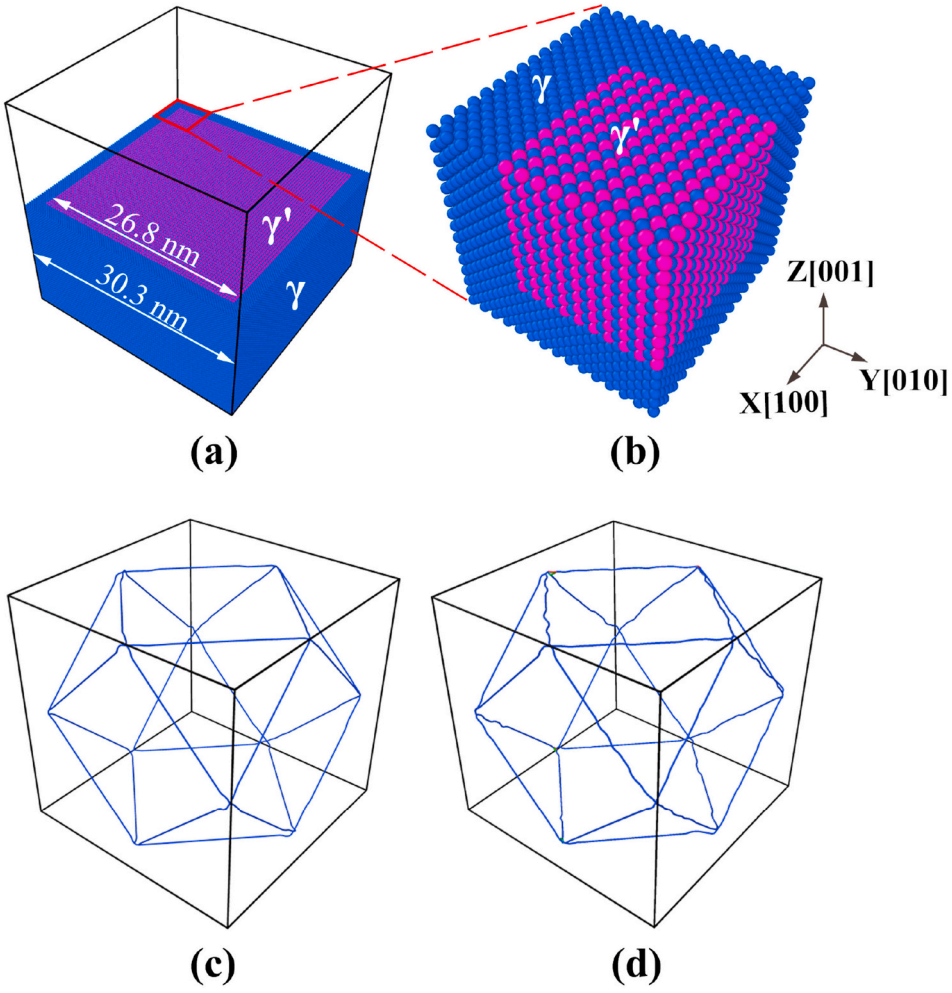

Fig. 1. Geometry of the atomic model for the Ni-based SC superalloy. (a) 3D view of the γ/γ' model with upper half being removed for clarity. (b) Enlarged local atomic environment of the γ/γ' interface, from the red box shown in (a). Ni and Al atoms are colored in blue and pink, respectively. Misfit dislocation networks formed on the γ/γ' interface after energy minimization of (c) pristine system and (d) 1 at.% Re system.

relatively smaller than the dimensions of γ and γ' phases in an experimental sample, which may affect quantitatively the magnitude of flow stress. However, the surveyed dislocation mechanisms are expected to be robust against variation in sample size. Fig. 1(b) shows the local atomic structure of γ/γ' interface. After energy minimization via conjugate gradient algorithm, 3D interfacial 1/2<110> perfect dislocation networks appear in Fig. 1(c).

The loading-unloading-reloading uniaxial tensile deformations are conducted along [100] direction at 300 K, with a constant strain rate of 10^8 s^{-1}. Isothermal-isobaric MD is performed within the Nosé-Hoover [33,34] and Parrinello-Rahman barostat [35]. The time step is 2 fs. Before deformation, the system has been relaxed to the thermodynamic equilibrium state. Because Re atoms mainly distribute into the γ phase in Ni-based SC superalloys [36,37], here 1 at.% Re atoms are randomly added into the γ phase as substitutions to replace the host Ni atoms. The concentration of Re is within the range of experimental superalloys [38]. Fig. 1(d) further shows the 3D pattern of the interfacial 1/2<110> perfect dislocation networks of the 1 at.% Re system after energy minimization. Compared with the pristine system, it can be seen that the local dislocation lines are slightly bent to be rough in the 1 at.% Re system, but the overall structure of the initial dislocation networks remains unchanged. Then the mechanical responses of the pristine and 1 at.% Re systems are compared to examine the alloying effect.

3. Results

MD simulations usually start with a defect-free atomic model which inevitably induces artificial mechanical response in contrast with experimental conditions. One of the drawbacks of a perfect model is the obscure stress overshoot and the following brute-force stress drop at yielding, which has something to do with unnecessary dislocation nucleation. While in experimental samples, the stress is a reflection of the resistance of pre-existing mobile dislocations. In this context, the artificial dislocation nucleation from a defect-free MD model bothers a correct understanding of the mechanical properties of materials from a simulation perspective. To create a relatively more experimentally relevant simulation model, we first perform a loading-unloading process to introduce a certain number of pre-existing dislocations for further reloading. During the loading process, the evolution of the interfacial dislocation networks is shown in Fig. 2. Fig. 2(a) shows the morphology of the dislocation networks just after the thermodynamic equilibrium at 300 K. Compared with athermal energy minimization, the dislocation networks have the tendency to change to cubic shape, and the dislocations in the γ channel begin to accumulate near the dislocation networks. At the strain of 1.2% in Fig. 2(b), the interfacial dislocation networks in the lower right corner have also evolved into a right-angle shape. The interfacial dislocation networks effectively prevent the dislocations in γ phase from shearing into γ' phase. At the strain of 2.0% in Fig. 2(c), the dislocation networks in the lower left corner have been damaged to a certain extent. As the loading continues, e.g., at the strain of 2.4% in Fig. 2(d), some dislocations in γ phase have bypassed the dislocation networks and sheared into the γ' phase. Moreover, in order to increase the reliability of the simulations, three independent samples with random 1 at.% Re substitution are considered. Fig. 3(a) shows the stress-strain curves of the pristine system and the three 1 at.% Re systems during the loading-unloading process at 300 K with strain rate of 10^8 s^{-1}. As shown in Fig. 3(a), after initial elastic stage, both of the two types of samples yield at around strain magnitude of ~3%, then stress evolves

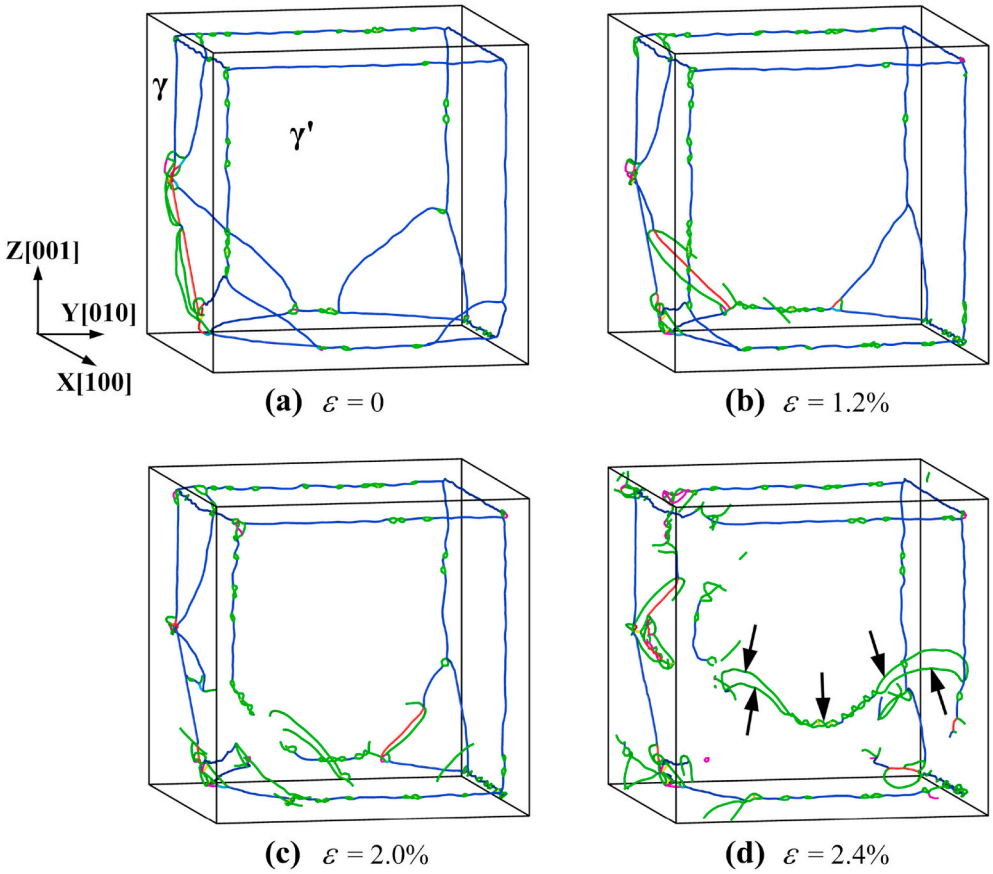

Fig. 2. The dislocation network morphologies of the pristine system at the strains of (a) 0, (b) 1.2%, (c) 2.0%, and (d) 2.4%, respectively, under a strain rate of 10^8 s^{-1} at 300 K. The dislocations indicated by the black arrows in (d) have sheared into γ' phase from γ phase. The color coding scheme: 1/2<110> Perfect (blue), 1/6<112> Shockley (green), 1/6<110> Stair-rod (pink), 1/3<001> Hirth (yellow), 1/3<111> Frank (light blue), and Others (red).

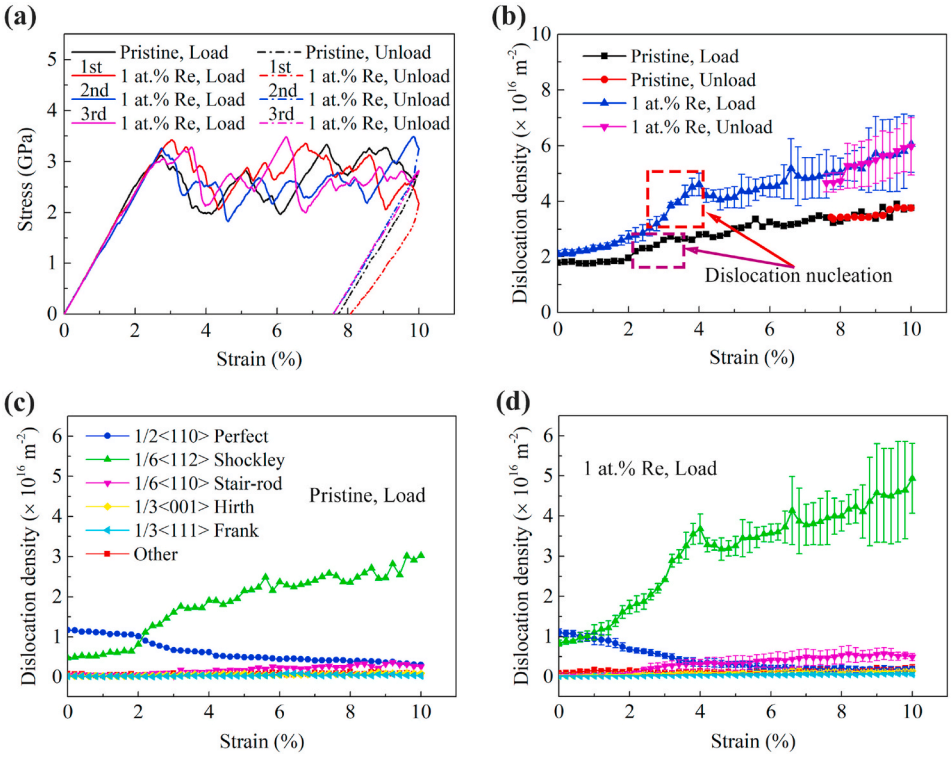

Fig. 3. Loading-unloading process of the pristine and 1 at.% Re systems, respectively, under a strain rate of 10^8 s^{-1} at 300 K. (a) The stress-strain curves. 1st, 2nd and 3rd indicate the three independent systems with random 1 at.% Re substitution. (b) Evolution of total dislocation densities versus strain. Evolution of densities of different types of dislocations in the loading process of (c) pristine system, and (d) 1 at.% Re system, respectively. The dislocation density of the 1 at.% Re system is the statistical average of three independent systems with random 1 at.% Re substitution. The error bars indicate standard deviation.

into steady state with pronounced fluctuations.

As illustrated by red and purple boxes in Fig. 3(b), the huge stress overshoots at yielding are corresponding to the remarkable dislocation nucleation which obviously increases dislocation density. Here, the dislocation density of the 1 at.% Re system is given by statistically averaging the dislocation densities of the three independent samples with random 1 at.% Re substitution. The error bars denote the fluctuating flow stress due to random Re substitution. During loading, the dislocation density of the 1 at.% Re system is greater than that of the pristine system. In other words, addition of Re facilitates the dislocation nucleation and increases the dislocation density, which would later increase the possibility of forest dislocation strengthening and extra work hardening ability of the Ni–Al-Re superalloy. Once we break down the total dislocation density to different categories in Fig. 3(c and d), it is found the Re addition mainly promotes extra 1/6<112> partial dislocations which are mobile under loading. More interestingly, the 1/6<110> stair-rod dislocations are invoked more with Re addition which will definitely affect the mechanics since its sessile nature. Table 1 lists the densities of different types of dislocations at the strain of 10% in the loading process for the pristine and 1 at.% Re systems, respectively. Except the type of 1/2<110> perfect, it can be seen that the dislocation densities of the remaining types in 1 at.% Re system are greater than those in pristine system. Note that the samples after loading-unloading process have dislocation density of the order of ~10^{16} m^{-2}, which is two or three orders of magnitude higher than the experimental samples with dislocation density of 10^{13}–10^{14} m^{-2} [39]. Yet the pre-existing dislocation samples in simulations are more experimentally relevant than the defect-free samples, which is expected to deduce more meaningful mechanical behaviors.

Table 1
Densities of different types of dislocations at the strain of 10% in the loading process for the pristine and 1 at.% Re systems, respectively, under a strain rate of 10^8 s^{-1} at 300 K.

	Dislocation density (× 10^{16} m^{-2})	
	Pristine system	1 at.% Re system
1/2<110> Perfect	0.31	0.20
1/6<112> Shockley	3.02	4.94
1/6<110> Stair-rod	0.26	0.49
1/3<001> Hirth	0.09	0.15
1/3<111> Frank	0.03	0.06
Other	0.06	0.21

Then we perform reloading on the models with pre-existing dislocations after loading-unloading operation. The mechanical information and dislocation information are displayed in Fig. 4. Fig. 4(a) shows the stress-strain curves of the pristine and the three independent 1 at.% Re systems, respectively. From the flow stress window between the yielding point and 20% strain, we estimate the values of flow stresses and show the data in the inset of Fig. 4(a), where the flow stress of the 1 at.% Re system is estimated by statistics on the all the flow stress data between the yielding point and 20% strain for all the three independent 1 at.% Re systems. It is found that an addition of 1 at.% Re effectively increases the flow stress from 2.7 GPa to 2.8 GPa, taking account the stress fluctuation as indicated by the error bars, which is in accordance with the common sense that Re strengthens nickel-based superalloys from experimental observations [10].

Looking at the total and the decomposed dislocation densities (in which the dislocation density of 1 at.% Re system is given by statistical value of the three independent 1 at.% Re systems) as shown in Fig. 4 (b–d), it is concluded that Re addition also promotes dislocation multiplication during reloading process and therefore increases the possibility of work hardening owing to the mechanism of forest dislocation strengthening. For example, after reloading to strain 20%, the 1 at.% Re sample has dislocation density of 1.28 × 10^{17} m^{-2}, which is greater than that of Re-free sample with dislocation density 1.11 × 10^{17} m^{-2}. Table 2 lists the densities of different types of dislocations at the strain of 20% in the reloading process for the pristine and 1 at.% Re systems, respectively. Except the types of 1/3<001> Hirth and others, the dislocation densities of the remaining types in 1 at.% Re system are greater than those in pristine system. Specifically, the 1/6<112> partials increase by 18.99%, and 1/6<110> stair-rod dislocations increase by 6.88% with 1 at.% Re addition, respectively. In both systems, 1/6<112> partials and

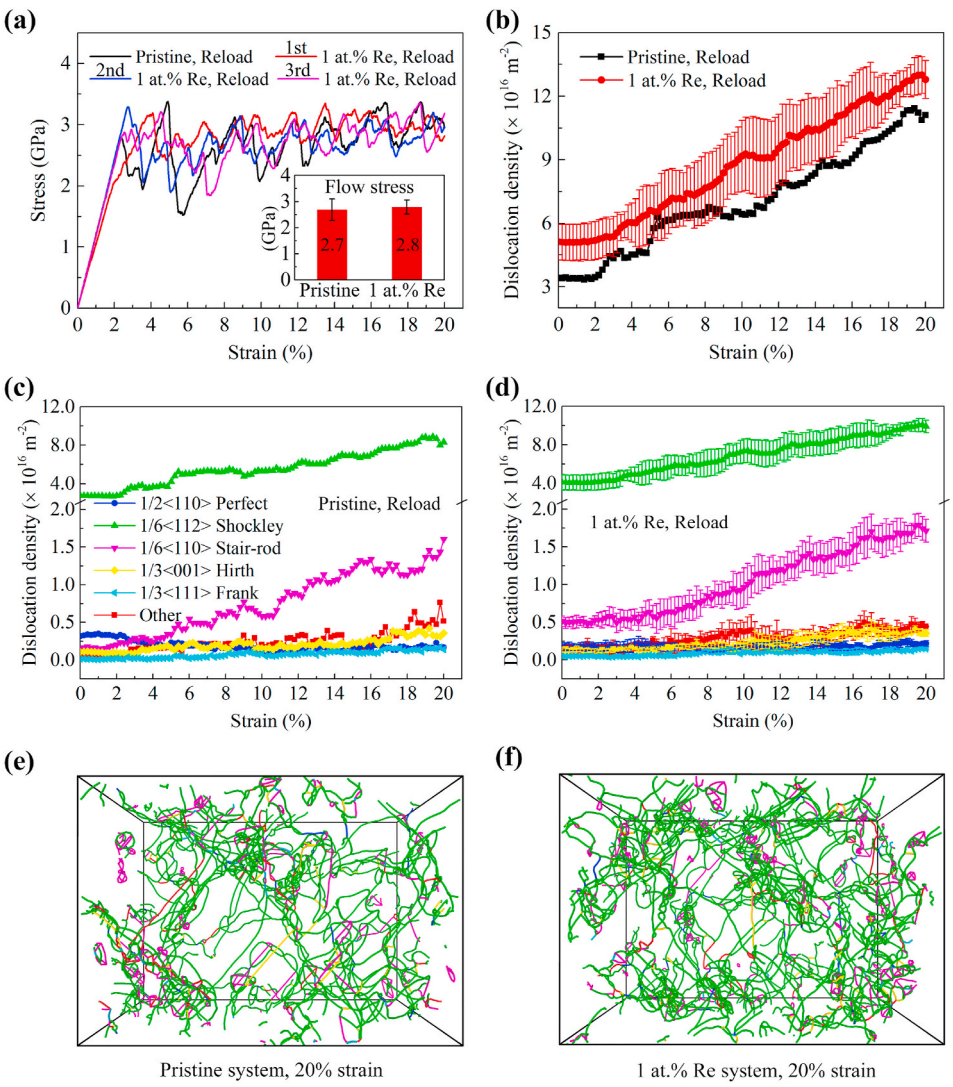

Fig. 4. Reloading process of the pristine and 1 at.% Re systems, respectively. (a) The stress-strain curves. 1st, 2nd and 3rd indicate the three independent systems with random 1 at.% Re substitution. The inset shows the average flow stresses of the pristine and 1 at.% Re systems, respectively, determined from the flow stress window between the yielding point and 20% strain. (b–d) Evolution of total dislocation densities and those of different types of dislocations in both pristine and 1 at.% Re systems, respectively. The dislocation patterns after 20% strain are shown in (e) pristine system, and (f) 1 at.% Re system, respectively. The error bars in (b) and (d) denote standard deviation. The color coding scheme in (e, f): 1/2<110> Perfect (blue), 1/6<112> Shockley (green), 1/6<110> Stair-rod (pink), 1/3<001> Hirth (yellow), 1/3<111> Frank (light blue), and Others (red).

Table 2
Densities of different types of dislocations at the strain of 20% in the reloading process for the pristine and 1 at.% Re systems, respectively, under a strain rate of 10^8 s^{-1} at 300 K.

	Dislocation density (× 10^{16} m^{-2})	
	Pristine system	1 at.% Re system
1/2<110> Perfect	0.17	0.22
1/6<112> Shockley	8.32	9.90
1/6<110> Stair-rod	1.60	1.71
1/3<001> Hirth	0.36	0.36
1/3<111> Frank	0.14	0.15
Other	0.52	0.44

1/6<110> stair-rod dislocations play important roles in the deformation and strengthening. To stress the uniqueness of Re in strengthening Ni-based superalloys, we compare the mechanics and dislocation behaviors in the test Ni–Al-Re and Ni–Al–Co systems, as shown in the Fig. S1 and Table S1 in the supplementary material. It is concluded that, at the same strain rate and substitutional positions, Re provides extra strengthening with higher values of both mobile (1/6<112> Shockley) and sessile (1/6<110> Stair-rod) dislocation densities. Fig. 4(e and f) shows the spatial distribution of all the dislocations. One impressed feature of the dislocation patterns is that there are great opportunities to see the 1/6<112> partials bundled with 1/6<110> stair-rod dislocations, which drives us to further uncover the strengthening mechanisms with the roles of either Re-dislocation interaction, or dislocation-dislocation interaction.

4. Discussion

Here we discuss the possible strengthening mechanisms of Re in superalloys. Further zoom in of the dislocation behaviors are summarized in Figs. 5 and 6. Fig. 5 shows one scenario of the interaction between the 1/6<110> stair-rod dislocations and the 1/6<112> Shockley partial dislocations during reloading. At the strain of 2.2%, the top mobile partial dislocations move toward the immobile stair-rod dislocations (see Fig. 5(a)). At the strain of 2.3%, the top mobile partial dislocations move closer to the immobile stair-rod dislocations, as shown in Fig. 5(b). At a later stage of strain magnitude of 2.4%, the stair-rod dislocations have trapped the top Shockley partials (see Fig. 5(c)). From the strain interval of 2.5%–2.7%, the motion of the Shockley partials has been effectively blocked by the stair-rod dislocations (see Fig. 5(d–f)). The pinning effect of the stair-rod dislocations on the mobile dislocations, to some extent, can strengthen the superalloys and improve the creep resistance.

Moreover, Fig. 6 displays a set of typical snapshots of the solid solution strengthening mechanism, with the role of dislocation motion interrupted by Re atoms, as is shown in Fig. 6(a and b). Even sometimes

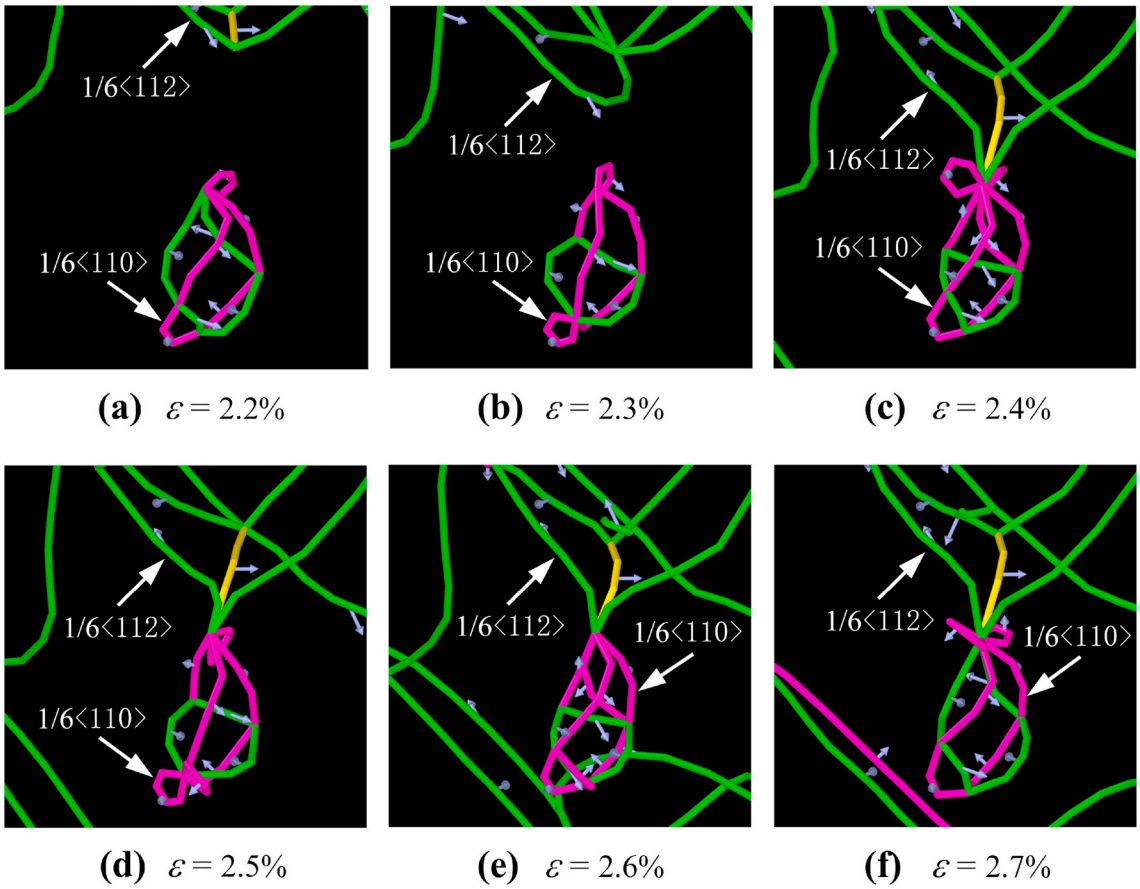

Fig. 5. The process of the interaction between the sessile 1/6<110> (Stair-rod) and the glissile 1/6<112> (Shockley) dislocations, in which the former blocks the motion and traps the latter dislocations. The dislocation color coding scheme is identical to those in Fig. 4(e and f). A supplementary movie is accompanied with the snapshots (see Movie S1 in the supplementary material).

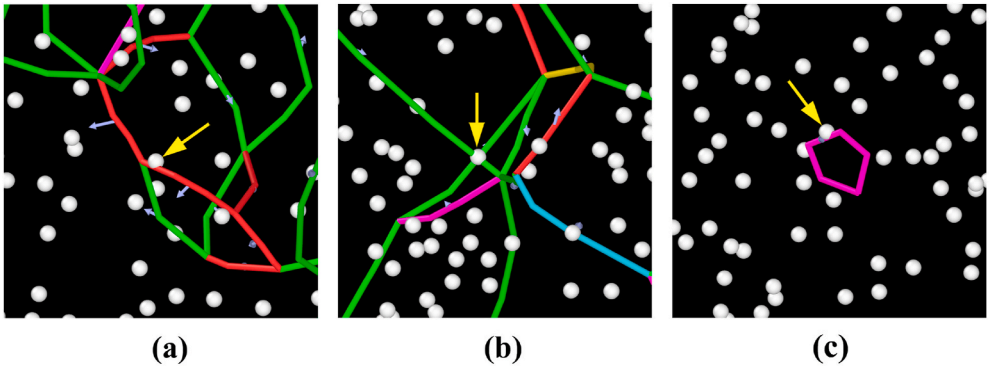

Fig. 6. Solid solution mechanism, in which Re impedes the motion of versatile mobile dislocations. The dislocation color coding scheme is identical to those in Fig. 4 (e and f). The white balls represent the Re atoms. Yellow arrows locate the exact Re atoms pinning the mobile dislocations.

dislocation loops are left after dislocation interaction with solid solution atom, as shown in Fig. 6(c), which is an evidence of the mechanism of solid solution strengthening.

5. Conclusion

In summary, through developing a loading-unloading-reloading protocol, we investigate the microscopic mechanism of Re strengthening in Ni-based superalloys by atomistic simulations. By analyzing the atomic-scale dislocation density evolution and the details of spatial nature of versatile dislocations, we put down the increased flow stress with Re addition to three basic mechanisms. First comes the usual solid solution mechanism due to the interaction between Re and mobile dislocations. The second interesting mechanism unveiled is the extra work hardening due to Re-assisted rapid dislocation nucleation and increased density that encourages forest dislocation interaction. Finally, Re atoms promote more 1/6<110> stair-rod dislocations upon loading which are sessile and, therefore, will act as obstacles for the glissile 1/6<112> Shockley partial dislocations. The three mechanisms synergistically help Re addition improve the mechanical properties of the Ni-based superalloys. Finally, we note that the present simulations at ambient temperature and the short MD timescale miss diffusive mechanism that

accommodates the creep deformation of superalloys at the elevated temperature service condition, which also involves mechanism of dislocation climb driven by vacancy diffusion in the vicinity of dislocation core. Therefore, a further investigation of the role of Re addition in creep will move another step toward understanding the high-temperature strengthening mechanisms, which deserves a future study.

Data availability

The raw/processed data required to reproduce these findings cannot be shared at this time due to legal or ethical reasons.

CRediT authorship contribution statement

En-Lai Yue: Conceptualization, Methodology, Software, Formal analysis, Writing - original draft, Writing - review & editing. **Tao Yu:** Conceptualization, Writing - review & editing, Funding acquisition. **Yun-Jiang Wang:** Conceptualization, Writing - review & editing, Funding acquisition. **Chong-Yu Wang:** Project administration, Funding acquisition.

Declaration of competing interest

The authors declare that they have no known competing financial interests or personal relationships that could have appeared to influence the work reported in this paper.

Acknowledgements

This work was financially supported by the National Key Research and Development Program of China (Grant No. 2017YFB0701502, and Grant No. 2017YFB0701503), the NSFC (Grant No. 11672299, and Grant No. 12072344), and the Youth Innovation Promotion Association of Chinese Academy of Sciences (Grant No. 2017025). Simulations were performed on the "Explorer 100" cluster system of Tsinghua National Laboratory for Information Science and Technology, Beijing, China.

Supplementary data

Supplementary data to this article can be found online at https://doi.org/10.1016/j.intermet.2021.107133.

References

[1] R.C. Reed, The Superalloys: Fundamentals and Applications, Cambridge University Press, Cambridge, 2006.
[2] T.M. Pollock, S. Tin, Nickel-based superalloys for advanced turbine engines: chemistry, microstructure and properties, J. Propuls. Power. 22 (2006) 361–374.
[3] T.M. Smith, B.D. Esser, N. Antolin, A. Carlsson, R.E.A. Williams, A. Wessman, T. Hanlon, H.L. Fraser, W. Windl, D.W. McComb, Phase transformation strengthening of high-temperature superalloys, Nat. Commun. 7 (2016) 1–7.
[4] A. Heckl, S. Neumeier, M. Göken, R.F. Singer, The effect of Re and Ru on γ/γ′ microstructure, γ-solid solution strengthening and creep strength in nickel-base superalloys, Mater. Sci. Eng. A. 528 (2011) 3435–3444.
[5] S. Wöllmer, T. Mack, U. Glatzel, Influence of tungsten and rhenium concentration on creep properties of a second generation superalloy, Mater. Sci. Eng. A. 319 (2001) 792–795.
[6] T.M. Pollock, R.D. Field, Dislocations and high-temperature plastic deformation of superalloy single crystals, in: Dislocations in Solids, Elsevier, 2002, pp. 547–618.
[7] M. Huang, Z. Cheng, J. Xiong, J. Li, J. Hu, Z. Liu, J. Zhu, Coupling between Re segregation and γ/γ′ interfacial dislocations during high-temperature, low-stress creep of a nickel-based single-crystal superalloy, Acta Mater. 76 (2014) 294–305.
[8] A. Mottura, M.W. Finnis, R.C. Reed, On the possibility of rhenium clustering in nickel-based superalloys, Acta Mater. 60 (2012) 2866–2872.
[9] P. Caron, T. Khan, Evolution of Ni-based superalloys for single crystal gas turbine blade applications, Aero. Sci. Technol. 3 (1999) 513–523.
[10] A.C. Yeh, S. Tin, Effects of Ru and Re additions on the high temperature flow stresses of Ni-base single crystal superalloys, Scripta Mater. 52 (2005) 519–524.
[11] X. Zhang, C.Y. Wang, First-principles study of vacancy formation and migration in clean and Re-doped γ′-Ni_3Al, Acta Mater. 57 (2009) 224–231.
[12] M.S.A. Karunaratne, P. Carter, R.C. Reed, Interdiffusion in the face-centred cubic phase of the Ni–Re, Ni–Ta and Ni–W systems between 900 and 1300°C, Mater. Sci. Eng. A. 281 (2000) 229–233.
[13] A. Janotti, M. Krčmar, C.L. Fu, R.C. Reed, Solute diffusion in metals: larger atoms can move faster, Phys. Rev. Lett. 92 (2004) 85901.
[14] M.S.A. Karunaratne, R.C. Reed, Interdiffusion of the platinum-group metals in nickel at elevated temperatures, Acta Mater. 51 (2003) 2905–2919.
[15] X.X. Yu, C.Y. Wang, The effect of alloying elements on the dislocation climbing velocity in Ni: A first-principles study, Acta Mater. 57 (2009) 5914–5920.
[16] S.H. Liu, C.P. Liu, L. Ge, X.N. Zhang, T. Yu, P. Yan, C.Y. Wang, Effect of interactions between elements on the diffusion of solutes in Ni-X-Y systems and γ′-coarsening in model Ni-based superalloys, Scripta Mater. 138 (2017) 100–104.
[17] L.T. Mushongera, M. Fleck, J. Kundin, Y. Wang, H. Emmerich, Effect of Re on directional γ′-coarsening in commercial single crystal Ni-base superalloys: A phase field study, Acta Mater. 93 (2015) 60–72.
[18] Q.Q. Ding, S.Z. Li, L.Q. Chen, X.D. Han, Z. Zhang, Q. Yu, J. Li, Re segregation at interfacial dislocation network in a nickel-based superalloy, Acta Mater. 154 (2018) 137–146.
[19] X.X. Wu, S.K. Makineni, C.H. Liebscher, G. Dehm, J.R. Mianroodi, P. Shanthraj, B. Svendsen, D. Bürger, G. Eggeler, D. Raabe, Unveiling the Re effect in Ni-based single crystal superalloys, Nat. Commun. 11 (2020) 1–13.
[20] J. Amodeo, C. Begau, E. Bitzek, Atomistic simulations of compression tests on Ni_3Al nanocubes, Mater. Res. Lett. 2 (2014) 140–145.
[21] A. Prakash, J. Guénolé, J. Wang, J. Müller, E. Spiecker, M.J. Mills, I. Povstugar, P. Choi, D. Raabe, E. Bitzek, Atom probe informed simulations of dislocation–precipitate interactions reveal the importance of local interface curvature, Acta Mater. 92 (2015) 33–45.
[22] E. Bitzek, P. Gumbsch, Mechanisms of dislocation multiplication at crack tips, Acta Mater. 61 (2013) 1394–1403.
[23] Y.J. Wang, G.J.J. Gao, S. Ogata, Size-dependent transition of deformation mechanism, and nonlinear elasticity in Ni_3Al nanowires, Appl. Phys. Lett. 102 (2013) 41902.
[24] Y.J. Wang, K. Tsuchiya, L.H. Dai, Size-dependent plastic deformation and failure mechanisms of nanotwinned Ni_3Al: insights from an atomistic cracking model, Mater. Sci. Eng. A. 649 (2016) 449–460.
[25] S. Plimpton, Fast parallel algorithms for short-range molecular dynamics, J. Comput. Phys. 117 (1995) 1–19.
[26] J.P. Du, C.Y. Wang, T. Yu, Construction and application of multi-element EAM potential (Ni–Al–Re) in γ/γ′ Ni-based single crystal superalloys, Model. Simulat. Mater. Sci. Eng. 21 (2013) 15007.
[27] S.L. Liu, C.Y. Wang, T. Yu, Influence of the alloying elements Re, Co and W on the propagation of the Ni/Ni_3Al interface crack, RSC Adv. 5 (2015) 52473–52480.
[28] Z.G. Liu, C.Y. Wang, T. Yu, Influence of Re on the propagation of a Ni/Ni_3Al interface crack by molecular dynamics simulation, Model. Simulat. Mater. Sci. Eng. 21 (2013) 45009.
[29] S.L. Liu, C.Y. Wang, T. Yu, Z.G. Liu, Effect of Re on lattice trapping in γ′-Ni_3Al cracks by atomistic simulation, Comput. Mater. Sci. 97 (2015) 102–108.
[30] A. Stukowski, Visualization and analysis of atomistic simulation data with OVITO–the Open Visualization Tool, Model. Simulat. Mater. Sci. Eng. 18 (2009) 15012.
[31] T. Zhu, C.Y. Wang, Misfit dislocation networks in the γ/γ′ phase interface of a Ni-based single-crystal superalloy: molecular dynamics simulations, Phys. Rev. B. 72 (2005) 14111.
[32] X.P. Tan, J.L. Liu, X.P. Song, T. Jin, X.F. Sun, Z.Q. Hu, Measurements of γ/γ′ Lattice Misfit and γ′ Volume Fraction for a Ru-containing Nickel-based Single Crystal Superalloy, J. Mater. Sci. Technol. 27 (2011) 899–905.
[33] S. Nosé, A molecular dynamics method for simulations in the canonical ensemble, Mol. Phys. 52 (1984) 255–268.
[34] W.G. Hoover, Canonical dynamics: equilibrium phase-space distributions, Phys. Rev. A. 31 (1985) 1695–1697.
[35] M. Parrinello, A. Rahman, Polymorphic transitions in single crystals: A new molecular dynamics method, J. Appl. Phys. 52 (1981) 7182–7190.
[36] A. Volek, F. Pyczak, R.F. Singer, H. Mughrabi, Partitioning of Re between γ and γ′ phase in nickel-base superalloys, Scripta Mater. 52 (2005) 141–145.
[37] R.C. Reed, A.C. Yeh, S. Tin, S.S. Babu, M.K. Miller, Identification of the partitioning characteristics of ruthenium in single crystal superalloys using atom probe tomography, Scripta Mater. 51 (2004) 327–331.
[38] A. Mottura, R.T. Wu, M.W. Finnis, R.C. Reed, A critique of rhenium clustering in Ni–Re alloys using extended X-ray absorption spectroscopy, Acta Mater. 56 (2008) 2669–2675.
[39] X. Wu, P. Wollgramm, C. Somsen, A. Dlouhy, A. Kostka, G. Eggeler, Double minimum creep of single crystal Ni-base superalloys, Acta Mater. 112 (2016) 242–260.